UNCLASSIFIED

AD NUMBER

ADB176711

NEW LIMITATION CHANGE

TO

Approved for public release, distribution unlimited

FROM

Distribution authorized to DoD only; Critical Technology, Proprietary Info.; 18 Oct 93. Other requests shall be referred to DARPA, 3701 Fairfax Dr., Arlington, VA 22203-1714. This document contains export-controlled technical data.

AUTHORITY

DARPA ltr, 20 Nov 2001

THIS PAGE IS UNCLASSIFIED

UNCLASSIFIED

SECURITY CLASSIFICATION OF THIS PAGE

AD-B176 711

L(2)

REPORT DOCUMENTATION PAGE

Form Approved OMB No. 0704-0188

DTIC ELECTE OCT 18 1993 S U

1a. REPORT SECURITY CLASSIFICATION Unclassified	
2a. SECURITY CLASSIFICATION AUTHORITY N/A	3. DISTRIBUTION/AVAILABILITY OF REPORT Distribution Limited to DOD components only: Critical Technology Date PROPRIETARY INFORMATION
2b. DECLASSIFICATION/DOWNGRADING SCHEDULE N/A	
4. PERFORMING ORGANIZATION REPORT NUMBER(S) DARPA I 1993 Final Report	5. MONITORING ORGANIZATION REPORT NUMBER(S) 18 OCT 1993 N/A
6a. NAME OF PERFORMING ORGANIZATION Sandia Systems, Inc. 6b. OFFICE SYMBOL (If applicable) N/A	7a. NAME OF MONITORING ORGANIZATION DARPA U.S. Army Missile Command
6c. ADDRESS (City, State, and ZIP Code) 2655-A Pan American Freeway, NE Albuquerque, NM 87107	7b. ADDRESS (City, State, and ZIP Code) AMSMI-RD-WS-DP-SB Redstone Arsenal, AL 35898-5248
8a. NAME OF FUNDING/SPONSORING ORGANIZATION DARPA 8b. OFFICE SYMBOL (If applicable)	9. PROCUREMENT INSTRUMENT IDENTIFICATION NUMBER Contract #
8c. ADDRESS (City, State, and ZIP Code) 3701 Fairfax Drive Arlington, VA 22203-1714	10. SOURCE OF FUNDING NUMBERS PROGRAM ELEMENT NO.: N/A; PROJECT NO.: N/A; TASK NO.: N/A; WORK UNIT ACCESSION NO.: N/A

11. TITLE (Include Security Classification)

Overlay and Grating Line Shape Metrology Using Optical Scatterometry (unclassified)

12. PERSONAL AUTHOR(S)

Dr. Richard Krukar, Dr. John McNeil

13a. TYPE OF REPORT	13b. TIME COVERED	14. DATE OF REPORT (Year, Month, Day)	15. PAGE COUNT
Final	FROM 2/1/93 TO 8/1/93	931011	36

16. SUPPLEMENTARY NOTATION

WARNING: INFORMATION SUBJECT TO EXPORT CONTROL LAWS AND DESTRUCTION NOTICE

17. COSATI CODES		
FIELD	GROUP	SUB-GROUP

18. SUBJECT TERMS (Continue on reverse if necessary and identify by block number)

overlay, grating, metrology, optical scatter, semiconductor sub-micron, CD, linewidth, sensors, process control

19. ABSTRACT (Continue on reverse if necessary and identify by block number)

This Phase I effort demonstrated the feasibility of using scatterometry to provide sensors for process control and overlay measurement for structures having sub-um linewidths (CDs). The processes which we investigated were poly-Si etch and W selective deposition, with particular attention directed toward application in a cluster tool environment. We analyzed structures having CDs of approx. 0.2 um, 0.35 um, and 0.5 um. We used simulation techniques to show that scatterometry is capable of monitoring teh width and height of the lines during these processes. The CD prediction error for all of the studied cases was between 0.4 and 4 nm, with the height prediction error in the range of 5 to 21 nm. These results can be improved by using sub-range prediction techniques. Overlay measurement error was found to be less than 0.5 nm for these cases. These results agree with experimental results obtained for similar line structures. In a Phase II effort we would verify these simulations by constructing scatterometers and implementing them on process reactors.

20. DISTRIBUTION/AVAILABILITY OF ABSTRACT ☐ UNCLASSIFIED/UNLIMITED ☐ SAME AS RPT. ☐ DTIC USERS	21. ABSTRACT SECURITY CLASSIFICATION unclassified
22a. NAME OF RESPONSIBLE INDIVIDUAL Don Savage Project Mgr	22b. TELEPHONE (Include Area Code) (205)955-6444 22c. OFFICE SYMBOL AMSMI-RD-WS-DP-SB

DD Form 1473, JUN 86 Previous editions are obsolete.

SECURITY CLASSIFICATION OF THIS PAGE

unclassified

The following notice applies to any unclassified (including originally classified and now declassified) technical reports released to "qualified U.S. contractors" under the provisions of DoD Directive 5230.25, Withholding of Unclassified Technical Data From Public Disclosure.

NOTICE TO ACCOMPANY THE DISSEMINATION OF EXPORT-CONTROLLED TECHNICAL DATA

1. Export of information contained herein, which includes, in some circumstances, release to foreign nationals within the United States, without first obtaining approval or license from the Department of State for items controlled by the International Traffic in Arms Regulations (ITAR), or the Department of Commerce for items controlled by the Export Administration Regulations (EAR), may constitute a violation of law.

2. Under 22 U.S.C. 2778 the penalty for unlawful export of items or information controlled under the ITAR is up to two years imprisonment, or a fine of $100,000, or both. Under 50 U.S.C., Appendix 2410, the penalty for unlawful export of items or information controlled under the EAR is a fine of up to $1,000,000, or five times the value of the exports, whichever is greater; or for an individual, imprisonment of up to 10 years, or a fine of up to $250,000, or both.

3. In accordance with your certification that establishes you as a "qualified U.S. Contractor", unauthorized dissemination of this information is prohibited and may result in disqualification as a qualified U.S. contractor, and may be considered in determining your eligibility for future contracts with the Department of Defense.

4. The U.S. Government assumes no liability for direct patent infringement, or contributory patent infringement or misuse of technical data.

5. The U.S. Government does not warrant the adequacy, accuracy, currency, or completeness of the technical data.

6. The U.S. Government assumes no liability for loss, damage, or injury resulting from manufacture or use for any purpose of any product, article, system, or material involving reliance upon any or all technical data furnished in response to the request for technical data.

7. If the technical data furnished by the Government will be used for commercial manufacturing or other profit potential, a license for such use may be necessary. Any payments made in support of the request for data do not include or involve any license rights.

8. A copy of this notice shall be provided with any partial or complete reproduction of these data that are provided to qualified U.S. contractors.

DESTRUCTION NOTICE

For classified documents, follow the procedures in DoD 5200.22-M, Industrial Security Manual, Section II-19 or DoD 5200.1-R, Information Security Program Regulation, Chapter IX. For unclassified, limited documents, destroy by any method that will prevent disclosure of contents or reconstruction of the document.

OVERLAY AND GRATING LINE SHAPE METROLOGY USING OPTICAL SCATTEROMETRY: FINAL REPORT

August 31, 1993
Sponsored by
Defense Advanced Research Projects Agency (DOD)
Defense Small Business Innovation Research Program

ARPA Order No. 5916

Issued by the US. Army Missile Command Under
Contract #DAAH01-93-C-R027

Principal Investigator & Business Address:
Richard Krukar
SANDIA SYSTEMS, INC.
2655-A Pan American Freeway. NE
Albuquerque, NM 87107
505-343-8112

Effective Date of Contract: February 1, 1993; Contract Expiration Date: August 31, 1993
Reporting Period: 1 February, 1993 to 31 August 1993

DISCLAIMER

The views and conclusions contained in this document are those of the authors and should not be interpreted as representing the official policies, either express or implied, of the Defense Advanced Research Projects Agency or the US. Government.

Distribution limited to DOD components only: Critical Technology: September 1, 1993. Other requests for this document must be referred to Director, Defense Advanced Research Projects Agency, 3701 North Fairfax Drive, Arlington, VA 22203-1714.

WARNING:
INFORMATION SUBJECT TO EXPORT CONTROL LAWS

This document may contain information subject to the International Traffic in Arms Regulation (ITAR) or the Export Administration Regulation (EAR) of 1979 which may not be exported, released, or disclosed to foreign nationals inside or outside of the United States without first obtaining an export license. A violation of the ITAR or EAR may be subject to a penalty of up to 10 years imprisonment and a fine of $100,000 under U.S.C. 2778 or Section 2410 of the Export Administration Act of 1979. Include this notice with any reproduced portion of this document.

DESTRUCTION NOTICE

For unclassified documents, destroy by any method which precludes reconstruction of the document.

93 10

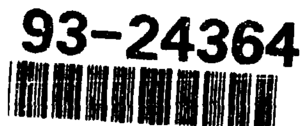

SBIR RIGHTS NOTICE (JUN 1987)

These SBIR data are furnished with SBIR rights under Contract No. DAAH01-93-C-R027. For a period of 2 years after acceptance of all items to be delivered under this contract, the Government agrees to use these data for Government purposed only, and they shall not be disclosed outside the Government (including disclosure for procurement purposes) during such period without permission of the Contractor, except that, subject to the foregoing use and disclosure prohibitions, such data may be disclosed for use by support Contractors. After the aforesaid 2-year period the Government has a royalty-free license to use, and to authorize others to use on its behalf, these data for Government purposes, but is relieved of all disclosure prohibitions and assumes no liability for unauthorized use of these data by third parties. This Notice shall be affixed to any reproductions of these data, in whole or part.

(End of Notice)

Accesion For
NTIS CRA&I
DTIC TAB
Unannounced
Justification
By
Distribution /
Availability Codes
Dist | Avail and / or Special
E-4

DTIC QUALITY INSPECTED 2

ABSTRACT

This Phase I effort demonstrated the feasibility of using scatterometry to provide sensors for process control and overlay measurement for structures having sub-μm linewidths (CDs). The processes which we investigated were etching poly-Si and selective deposition of W, with particular attention directed toward application in a cluster tool environment. We analyzed structures having CDs of ~0.20 μm, ~0.35 μm, and ~0.50 μm. We used simulation techniques to show that scatterometry is capable of monitoring the width and height of the lines during these processes, summarized as follows:

Structure	CD Prediction Error (nm)	Height Prediction Error (nm)
Si Etch, CD ~0.20 μm	**0.4**	**8**
Si Etch, CD ~0.35 μm	**3**	**21**
Si Etch, CD ~0.50 μm	**3**	**14**
W Depo., CD ~0.35 μm	**1**	**4**
W Depo., CD ~0.50 μm	**4**	**5**

These results can be improved by implementing the sub-range prediction techniques described. We have demonstrated the ability of scatterometry to provide overlay measurement in a simple manner which is summarized as follows:

OVERLAY MEASUREMENT ERROR: ≤ 0.5 nm

Note that we have applied these same simulation techniques in similar applications involving CDs in the range between 0.12 μm and 2 μm, and results have agreed well with experimental results. In a Phase II effort we would verify these simulations by constructing scatterometers and implementing them in reactors.

1.0 INTRODUCTION

The development of critical dimension (CD) metrology techniques has become crucial as the CDs of semiconductor devices have shrunk toward 0.25μm. The tolerances of the fabrication process, or error budget, are approximately 10% of the CD. The shrinking tolerances have led to the industry's steady drift from optical microscopy to scanning electron microscopy (SEM) [1] as the primary reference method for CD metrology. Additional CD metrology tools include scanning force microscopy (SFM) [2] and electrical linewidth measurements [3]. The critical performance issues with every metrology instrument are calibration, accuracy and precision [4]. Other desirable attributes are that the tool be non-contact, non-destructive, rapid and applicable *in-situ*. However, these three metrology techniques suffer from some combination of being slow, destructive, tedious, and unsuitable for *in-situ* application.

Optical scatterometry applied to periodic structures has all of the above attributes, and hence has tremendous potential as a CD metrology tool. Scatterometry consists of the measurement and analysis of light scattered from a sample surface [5]. In the case of a periodic structure, such as arrays or repetitive cells, the light is diffracted orders at angular locations specified by the grating equation

$$\sin\Theta_i + \sin\Theta_n = \frac{n\lambda}{d}, \qquad (1)$$

where Θ_i is the angle of incidence, Θ_n in the angular location of the n-th diffraction order, n is an integer, λ is the wavelength of incident radiation, and d is the period (pitch) of the structure. Figure 1 illustrates the geometry used in the description of diffraction.

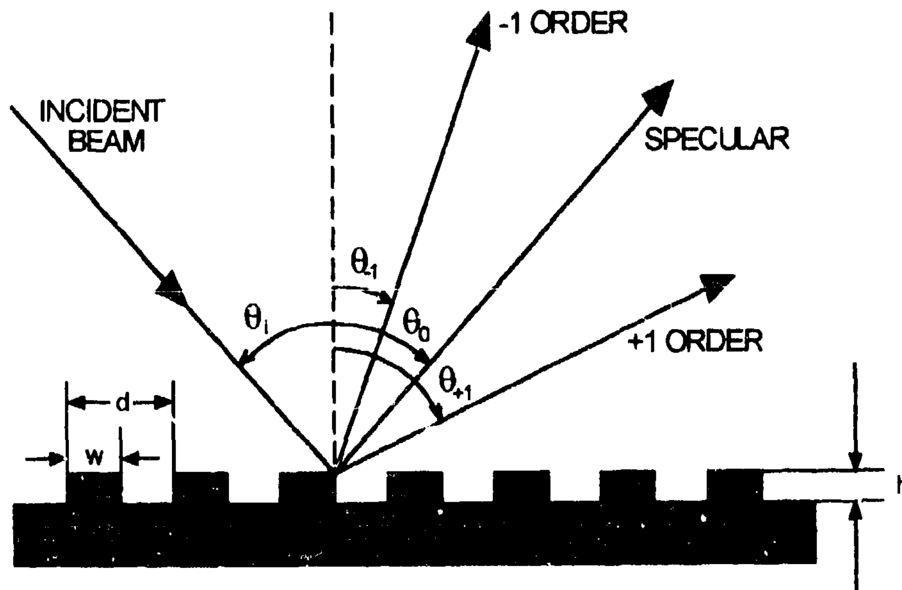

Figure 1: Diffraction geometry used in this effort

Information about the diffracting structure is obtained by interpreting the distribution of intensities in the various diffracted orders. This distribution is *extremely* sensitive to the width, height, and sidewall profile of the diffracting structure. Scatterometry is an optical metrology technique that does not suffer from the limitations of optical microscopy because, *unlike imaging*, the diffracted light is not combined or imaged prior to analysis.

When measuring diffraction from gratings, the polarization of the incident beam measurably affects the intensity of the diffracted beams. For TE polarization, the incident E field is parallel to the grating lines. When the E field is perpendicular to the grating lines, the beam is TM polarized. Typically we use TE polarization, although the polarization may be changed in a controlled manner to increase the amount of information obtained from a measurement.

For a fixed angle of incidence of the laser beam, the number of diffracted orders is determined by the ratio λ/d. The larger this ratio is, the greater the number of diffraction orders, and consequently, the greater the information content of the scatterometry data.

For small pitch structures in which the period of the grating is comparable to the wavelength of the incident probe beam as illustrated in Figure 1, only a few propagating diffraction orders exist. When the angle of incidence is fixed, little information is available from a scatterometer measurement, and alternative measurement arrangements must be implemented. Either the angle of incidence or the wavelength of the incident beam (or both) can be scanned, and the intensity of one or more diffraction orders can be continuously monitored. For this Phase I effort we demonstrated the feasibility of scatterometers which incorporate these two techniques; this is discussed in Section 2.

The behavior of the diffracted fields and their dependence on the diffracting structure lineshape can be understood using a rigorous formalism. A formalism we have used with great success to simulate and interpret diffraction data encountered using scatterometry is rigorous coupled wave theory (RCWT) [6]. RCWT numerically solves Maxwell's equations for the case of an incident wave illuminating a periodic structure. It is a first-principles solution of the diffraction problem and is therefore quantitative and accurate. Use of RCWT allows for the theoretical solution of the *forward grating diffraction problem*, that of predicting the distribution of intensities in the various diffraction orders when a laser beam is incident on a grating of *known* shape.

The *inverse grating diffraction problem*, predicting the lineshape of the diffracting structure from knowledge of the diffracted light characteristics, is quite difficult. This is because the diffraction characteristics vary in a complex, non-intuitive manner as the

lineshape of the diffracting structure is changed. The inverse problem has been a topic of active research for many years. Our approach to this has involved multivariate statistical techniques (e.g. Chemometrics) and has provided very good results. These same statistical techniques have been applied in this Phase I effort and are described in Section 2. Diffracted Scatter Analysis (DSA) [7], used for the solution of the inverse problem, combines scatterometry, theoretical simulation, and statistical analysis to predict critical dimensions from a measured optical scatter pattern.

2.0 OVERVIEW OF OUR APPLICATION OF SCATTEROMETRY TO PROCESS CONTROL AND OVERLAY MEASUREMENT

As explained previously, for a diffracting structure in which the pitch (and CD) of the diffracting structure is small compared to the incident probe beam wavelength, the angle of incidence or the wavelength can be varied in order to obtain a large amount of information in a measurement. A "2-Θ" scatterometer is the name applied to the arrangement in which the angle of incidence is scanned, and a "λ-scan" scatterometer is the name applied to the other situation in which the wavelength of the incident probe beam is scanned. In these two situations, the shapes of the curves that are obtained are *extremely sensitive* to the lineshape of the diffracting structure. Figures 2 and 3 illustrate the two scatterometer arrangements. In a Phase II effort we would construct and implement practical versions of these scatterometers which have no moving parts and other improvements which make them more amenable to fab line (cluster tool) use.

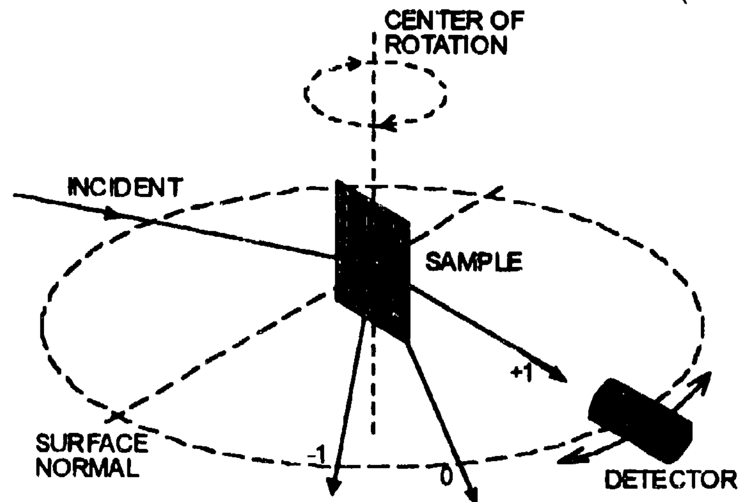

Figure 2. A 2-θ scatterometer which measures the power of a diffracted order as a function of incident angle.

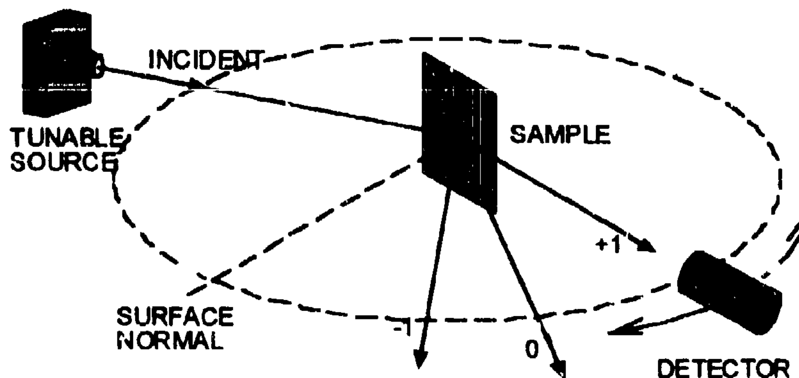

Figure 3. A λ-scan scatterometer which measures the power of a diffracted order as a function of incident wavelength.

We first identified two critical processes used in a cluster tool environment that require sensors for process control: poly-Si etch and selective deposition of W; additional details for this decision are discussed below. The RCWT approach was used to theoretically generate the scatter patterns corresponding to the 2-Θ and λ-scan scatterometer arrangements over a parameter space defined by expected variation of linewidth and height of the structure. The wavelength used for the probe beam for the 0.20 μm geometry was 325 nm, and 633 nm was used for the 0.35 μm and 0.50 μm geometries. The effects of process variations were simulated by allowing the height and width of the lines to vary around their nominal values.

A similar approach was taken for overlay measurement. The structure which was investigated consisted of two gratings. One grating had Si lines and SiO_2 spaces, and the other grating consisted of developed photoresist and was located on top of the Si/SiO_2 grating. The two gratings were modeled to have the same pitch but were offset from each other by different amounts. The wavelength of the probe beam used in these simulations was 633 nm. Additional details are given in Section 4.

The theoretical scatter patterns provided the calibration, or reference set of data needed to train the multivariate statistical analysis technique. This was used to solve the inverse problem of predicting the lineshape and overlay. We used partial least squares (PLS) for this purpose [7,8].

Cross validation was used to quantify the expected performance of a scatterometer and analysis technique when applied to a specific structure. Cross validation is the process of repeatedly calibrating the statistical technique using a subset of the calibration data, using the rest of the calibration data as "unknowns" which are submitted to the statistical technique for prediction, and recording the prediction error for each "unknown". The standard deviation of the prediction errors is the standard error of prediction (SEP) of the proposed instrument; i.e. the SEP values listed in the sections below represent the 1-σ precision of predicting the parameters of interest.

We calculated the SEP for three different noise situations for most applications. The first situation assumes that both the calibration data and the measurement data are noise-free. The second situation assumes that only the measurement data contains noise. The third situation assumes that both the measurement data and the calibration data contain noise. Examining these three cases characterizes the noise immunity of the proposed instrument.

Our experience over the past five years investigating the diffraction from etched structures and other relief gratings has been that the 0-order and 1st-order diffracted beams are typically strong and able to be seen with the unaided eye. Because of this the measurements contain low noise levels, and a conservative simulation involves the second case described above. The simulated calibration data is practically noise free.

The noise model chosen was

$$I = I_0 + k*N*\mathrm{sqrt}(I_0) \quad , \tag{2}$$

where N is a zero mean unit variance Gaussian random variable, k is a constant modifier used to change the noise power, I_0 is the noise free measurement, and I is the noisy measurement. This noise model mimics electronic noise in the measurement system. The value k=0.002 was chosen to heavily degrade the weak signals (with $I_0 \sim 0.000008$) in the simulated measurement while leaving the stronger signals relatively intact. This added simulated dynamic range limitations to the experiments.

This approach, i.e. diffraction simulation using the RCWT coupled with multivariate statistical analysis (PLS), provides an excellent platform for instrument design. Simulation can precisely characterize the behavior of a prototype instrument before the instrument is fabricated. The characteristics of a proposed instrument, including the measurement accuracy and precision, are known prior to construction. An additional benefit of this method of design is that the instrument is calibrated in the design phase. Because the simulation program is based on first order principals, the final instrument calibration is well characterized and is independent of any commercially available calibration standard. We have used this same approach in similar applications in which the calculations and experimental verification were in close agreement, such as characterizing the lineshape of developed photoresist. See Reference 5, which is attached in Appendix 1.

3.0 CRITICAL DIMENSION METROLOGY

The first task we performed was to determine relevant applications for scatterometry in today's and tomorrow's microelectronics industry. We visited Applied Materials in Santa Clara, CA, TI in Dallas, TX, SC Technologies in Livermore, CA, and Sandia National Laboratories in Albuquerque, NM,. Representatives of Applied Materials and Tencor subsequently visited us in Albuquerque. We communicated with Novellus in Santa Clara, CA, Drytech in Wilmington, MA, and AT&T in Allentown, PA. These contacts reported or confirmed that etching poly-Si and filling trenches with W are presently relevant processes that would benefit from advanced metrology.

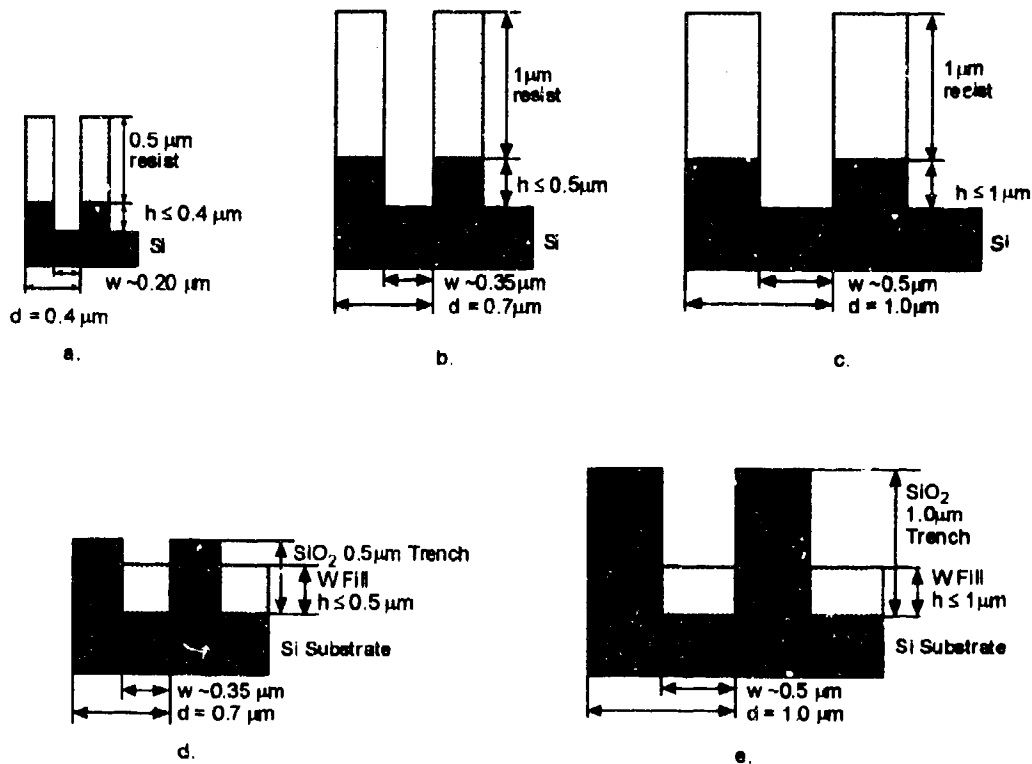

Figure 4. The five structures that were examined to demonstrate the applicability of scatterometry to monitor line shapes of etched poly-Si (parts a, b, and c) and deposited W (parts d and e).

Figure 4 shows the five specific structures we examined which correspond to two processes, with structures having nominal CDs of ~0.20 µm, ~0.35 µm, and ~0.50 µm. The poly-Si etching involved a photoresist mask that was 0.5 µm thick for the 0.2 µm CD structures, and 1.0 µm thick for the 0.35 µm and 0.50 µm structures. The selective W deposition process involved filling trenches in a SiO_2 grating over a Si substrate. The structures shown in Figures 4d and 4e show the trench partially filled with W. The second process was etching poly-Si through a photoresist mask.

The line width of the structures was varied by ±10% of the nominal value to accommodate for process variations that might occur. In addition, for each structure the size of the lines and spaces was approximately the same. This is realistic if issues involving proximity effects are to be avoided.

We emphasized 0.35 μm and 0.50 μm geometries in this effort because of their relevance to our Phase II effort which we will propose. Specifically, as discussed below, we will propose to implement a scatterometer on a deposition or etch system to monitor the process, and 0.20 μm geometries are not compatible with the systems available to us. In addition, the larger geometries represent a logical next step in the progression from current technology to smaller geometries. We will approach measuring 0.20 μm structures *ex-situ* as discussed in Section 7.

Figures 5, 6, and 7 show examples of data which we generated using RCWT. Figure 5 corresponds to the structure of Figure 4a (etched poly-Si and CD ~ 0.20 μm) and shows the variation of the 1st-order diffracted power with incident angle of the probe beam for three different line widths. Figure 6 corresponds to the structure of Figure 4b (etched poly-Si and CD ~ 0.35 μm) and shows the variation of the 1st-order diffracted power with incident wavelength of the probe beam for three line widths. Figure 7 corresponds to the structure of Figure 4d (selective W deposition and CD ~ 0.35 μm) and shows the variation of 0-order power with incident angle of the probe beam for three line heights. The differences between the three curves in each of the figures illustrates the sensitivity of the scatterometry technique to parameter changes, and this is what partial least squares exploits for prediction. Note that only three curves are included in each figure to avoid confusion that would occur if all the data were plotted.

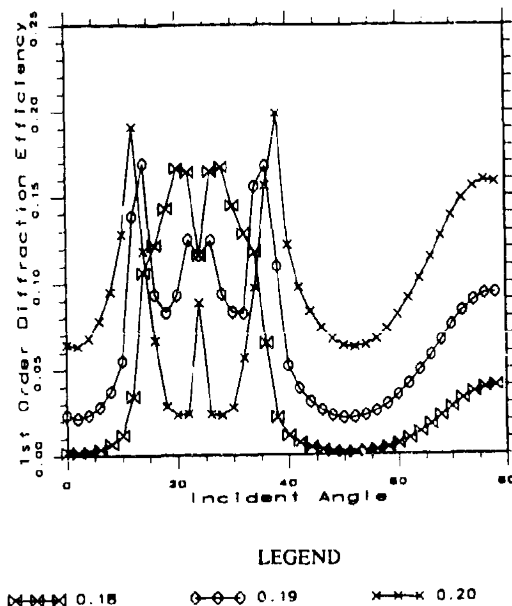

Figure 5: Simulated 2-Θ scatterometer data showing the 1st-order diffraction from characterizing an etched poly-Si structure of CD ~ 0.2 μm, for three different line widths; ledgend units are μm.

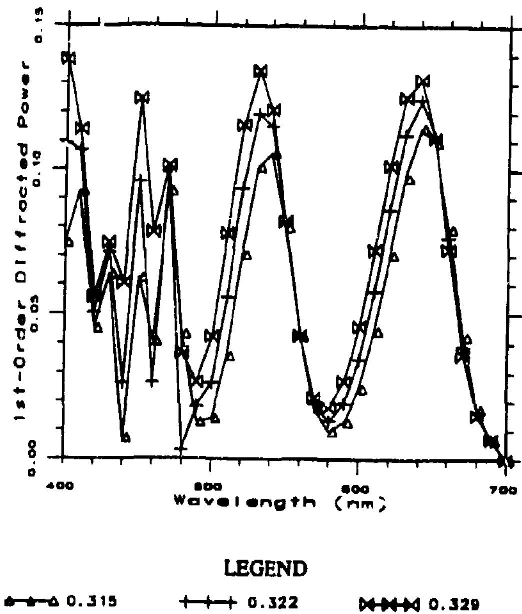

Figure 6: Simulated λ–Scan scatterometer data showing the 1st-order diffraction from characterizing an etched poly-Si structure of CD ~ 0.35 μm, for three different line widths; ledgend units are μm.

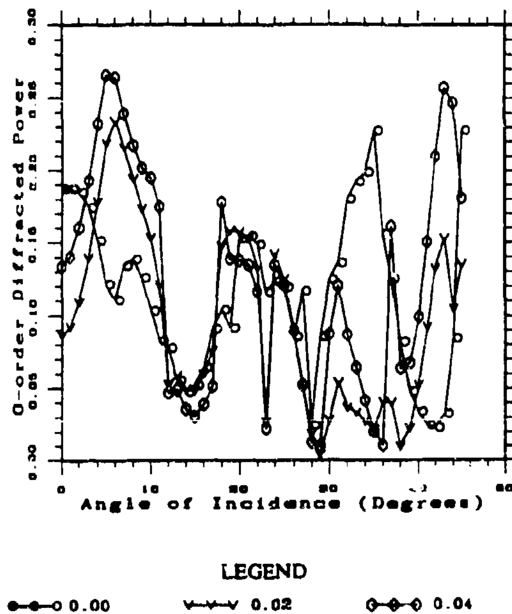

Figure 7: Simulated 2-Θ scatterometer data showing 0-order diffraction from characterizing selective W deposition structure of CD ~ 0.35 μm, for three different line heights; ledgend units are μm.

3.1 Si Etch, 0.20 μm CD

The 0.20/0.4 poly-Si etch structure is shown in Figure 4a which consists of a 0.5 μm thick photoresist grating mask over the poly-Si layer. The wavelength of the incident probe beam was 325 nm and TE polarization was used. The simulation started with a line height of 0.00 μm and continued until a line height of 0.40 μm was reached, increasing in increments of 0.02 μm, to simulate a total of 21 heights. The line width was varied by ±10% around the nominal width of 0.20 μm, in steps of 0.01 μm for a total of 5 widths. For this geometry the total number of simulations was 21x5=105. Each simulation consisted of a 2-Θ scan over the range of 0° to 78° for the angle of incidence, taken in steps of 2°. In this application we included noise in the measurement data and the calibration data (i.e., the third noise situation discussed in Section 2).

Table 1 shows the performance of the 2-Θ technique is very good at predicting the line width and the height. To improve on the height prediction, we implemented a technique called "sub-range analysis". This strategy first utilizes the full-range results of Table 1 to locate the line height to within 14 nm. This places the height into one of three sub-ranges: 0 nm to 200 nm, 100 nm to 300 nm, and 200 nm to 400 nm. The predictions for line height are then performed over the smaller sub-range to provide a significant improvement in the height SEP, as illustrated in Table 2.

Measurement Technique: 2-Θ	
Diffraction Order(s) Used:	0&1
Width SEP (nm) noise in measurement	0.4
Height SEP (nm) noise in measurement	14

Table 1. The SEPs for measuring critical dimensions of the 0.20/0.4 etched poly-Si structure using the full range of line height for prediction.

Sub-Range (nm):	0 - 200	100 - 300	200 - 400
Height SEP (nm):	1.3	2.5	8.5

Table 2. Sub-range analysis SEPs for line height prediction using unknown line width of the 0.20/0.40 etched poly-Si structure. A 2-Θ measurement technique and both diffraction orders were used for the analysis.

Note that this refinement in the analysis process does not involve any additional measurements and, because all the calibrations are already performed, can be computed

quickly. After training the PLS technique, the total analysis time required for prediction is on the order of a few msec. The sub-range process can be repeated to further improve prediction results. We are very pleased with this approach and have applied it to some of the other structures discussed below.

3.2 Si Etch, 0.35 μm CD

The 0.35/0.7 poly-Si etch structure is shown in Figure 4b. The process simulation began with a 1.0 μm thick photoresist grating over a poly-Si layer. The end point was when the poly-Si had been etched 0.5 μm deep. Simulations were run starting at the beginning and at .02 μm intervals until the 0.5 μm line height was obtained. The total number of etch heights was 26. The line width was varied ±10% around the nominal width. For the 0.35/0.7 structure, the range was 0.315 μm to 0.385 μm. A step size of 0.007 μm resulted in 11 different line widths. The total number of simulations was 26x11=281. The wavelength of the incident probe beam was 633 nm.

Measurement Technique:	2-θ			λ-scan		
Diffraction Order(s) Used:	0-order	1-order	0&1	0-order	1-order	0&1
Width SEP (nm) no noise	2	5	1	10	11	3
Width SEP (nm) noise in measurement	2	5	1	10	12	3
Width SEP (nm) noise in measurement & noise in calibration	3	6	1	10	11	3
Height SEP (nm) no noise	42	47	29	51	27	20
Height SEP (nm) noise in measurement	44	57	29	53	28	21
Height SEP (nm) noise in measurement & noise in calibration (nm)	43	56	29	52	27	21

Table 3. The SEPs (standard errors of prediction) for measuring critical dimensions of the 0.35/0.70 etched poly-Si structure.

The results shown in Table 3 indicate that the 0.35/0.7 Si etch structure can be predicted accurately using either arrangement, although the λ-scan technique provides slightly better results. The slight difference in the SEP of the predicted width from the two arrangements is inconsequential. The performance of both techniques could be improved using the sub-range technique described above in connection with the 0.20 μm structure.

3.3 Si Etch, 0.50 μm CD

The 0.5/1.0 poly-Si etch structure is shown in Figure 4c. The process simulation began with a 1.0 μm thick photoresist grating over a layer of poly-Si, representing a 0.0 μm deep etch. Simulations were run at .02 μm intervals until a line height of 1.0 μm was reached. The total number of line heights was 51. The line width was varied ±10% around the nominal width. For the 0.5/1.0 structure, the range was 0.45 μm to 0.55 μm. A step size of 0.01 μm resulted in 11 different line widths. The total number of simulations was 51x11=561. The wavelength of the incident probe beam was 633 nm.

Measurement Technique:	2-θ			λ-scan		
Diffraction Order(s) Used:	0-order	1-order	0&1	0-order	1-order	0&1
Width SEP (nm) no noise	5	5	2	6	8	3
Width SEP (nm) noise in measurement	5	6	2	6	8	3
Width SEP (nm) noise in measurement & noise in calibration	5	5	2	6	8	3
Height SEP (nm) no noise	241	257	209	278	273	227
Height SEP (nm) noise in measurement	244	277	215	279	273	227
Height SEP (nm) noise in measurement & noise in calibration (nm)	242	273	215	279	273	229

Table 4. The SEPs for measuring critical dimensions of the 0.5/1.0 poly-Si etch structure.

As Table 4 shows, the line width prediction results were excellent, but the height estimates were poor in all cases. Examination of the data revealed a periodic variation of the diffracted intensity with increasing line height. The variation is an interferometric effect of the optical path difference inside and outside the trench. The PLS analysis performs best when the measurement varies linearly with the critical dimension, and the solution quickly degrades when this is not the case. The PLS analysis is also poor when the measurement is not unique over the range of critical dimensions under study, as occurs here with periodic variations.

We then applied sub-range analysis described in Section 3.1 to improve the line height predictions. The height was divided into 5 overlapping sub-ranges between 0.0 μm and 1.0 μm, and the width was divided into 4 overlapping sub-ranges between 0.45 μm and 0.55 μm. The full-range results summarized in Table 4 were used to locate the prediction

into one of the 20 "bins" corresponding to a particular combination of width and height sub-ranges. We then applied PLS to determine the SEP for each sub-range. We used 0-order and 1st-order data in which the measurement data and the calibration data had noise (i.e. the third noise situation).

Tables 5 and 6 summarize the line height SEP obtained for each of the 20 "bins" using the 2-Θ technique and the λ-scan technique, respectively. It can be seen that the height prediction was significantly improved to provide SEPs that are less than 14 nm for the λ-scan technique and less than 36 nm for the 2-Θ technique. Thus the λ-scan technique is considered to provide the better overall performance for this specific application. We are very pleased with both of these results.

Linewidth & Height Ranges	0.45 – 0.49 (μm)	0.47 – 0.51 (μm)	0.49 – 0.53 (μm)	0.51 – 0.55 (μm)
0.0 – 0.36 (μm)	0.0053 μm	0.0061 μm	0.0083 μm	0.0086 μm
0.18 – 0.54 (μm)	0.0185 μm	0.0187 μm	0.0280 μm	0.0238 μm
0.36 – 0.72 (μm)	0.0220 μm	0.0255 μm	0.0225 μm	0.0213 μm
0.54 – 0.90 (μm)	0.0346 μm	0.0276 μm	0.0312 μm	0.0362 μm
0.72 – 1.00 (μm)	0.0199 μm	0.0061 μm	0.0138 μm	0.0099 μm

Table 5. Sub-range analysis SEPs for line height prediction using unknown line width of the 0.5/1.0 etched poly-Si structure. A 2-Θ measurement technique and both diffraction orders were used for the analysis.

Linewidth & Height Ranges	0.45 – 0.49 (µm)	0.47 – 0.51 (µm)	0.49 – 0.53 (µm)	0.51 – 0.55 (µm)
0.0 – 0.36 (µm)	0.0037 µm	0.0043 µm	0.0061 µm	0.0088 µm
0.18 – 0.54 (µm)	0.0094 µm	0.0086 µm	0.0137 µm	0.0118 µm
0.36 – 0.72 (µm)	0.0100 µm	0.0083 µm	0.0143 µm	0.0115 µm
0.54 – 0.90 (µm)	0.0145 µm	0.0135 µm	0.0101 µm	0.0095 µm
0.72 – 1.00 (µm)	0.0036 µm	0.0031 µm	0.0037 µm	0.0036 µm

Table 6. Sub-range analysis SEPs for line height prediction using unknown line width of the 0.5/1.0 etched poly-Si structure. A λ-scan measurement technique and both diffraction orders were used for the analysis.

3.4 Selective W Deposition, 0.35 µm CD

The 0.35/0.7 W deposition structure is shown in Figure 4d. The process simulation began with a 0.7 µm pitch, 0.5 µm deep SiO_2 grating over a bare Si wafer, representing a 0.0 µm W fill. Simulations were run starting at 0.0 µm and at .02 µm intervals until the 0.5 µm deep trench was completely filled. The total number of deposition heights was 26. The line width was also varied ±10 % around the nominal width to provide a range of 0.315 µm to 0.385 µm. A step size of 0.007 µm resulted in 11 different line widths. The total number of simulations was 26 x 11=286. The wavelength of the incident probe beam was 633 nm.

Measurement Technique:	2-θ			λ-scan		
Diffraction Order(s) Used:	0-order	1-order	0&1	0-order	1-order	0&1
Width SEP (nm) no noise	7	6	2	1	2	<1
Width SEP (nm) noise in measurement	8	7	2	2	3	1
Width SEP (nm) noise in measurement & noise in calibration	8	6	2	2	3	1
Height SEP (nm) no noise	6	16	4	5	6	2
Height SEP (nm) noise in measurement	8	24	4	8	15	4
Height SEP (nm) noise in measurement & noise in calibration (nm)	8	24	4	8	16	3

Table 7. The SEPs (standard errors of prediction) for measuring critical dimensions of the 0.35/0.7 W deposition structure.

Table 7 illustrates the predicted results for the 0.35/0.7 W deposition structure are exceptional for both scatterometer arrangements. The λ-scan technique slightly outperformed the 2-Θ technique for both the line width and height predictions. However, these differences are considered to be inconsequential. The 0-order column for the λ-scan arrangement suggests using a single fixed detector for the measurement, and this represents a simple instrument with no moving parts and easy alignment.

3.5 Selective W Deposition, 0.50 μm CD

The 0.5/1.0 W deposition structure is shown in Figure 4e. The process began with a 1.0 μm pitch, 1.0 μm deep SiO_2 grating over a bare Si wafer, representing a 0.0 μm W fill. Simulations were run at 0.0 μm and at .02 μm intervals until the 1.0 μm deep trench was completely filled. The total number of deposition heights was 51. The line width was varied ±10 % around the nominal width. For the 0.5/1.0 structure, the range was 0.45 μm to 0.55 μm. A step size of 0.01 μm resulted in 11 different line widths. The total number of simulations was 51x11=561. The wavelength of the incident probe beam was 633 nm.

Table 8 illustrates how the line width of the 0.5/1.0 W deposition structure can be quite well measured using either technique, although the λ-scan technique performs slightly better. The deposition height SEP for the 2-θ arrangement is marginal because the measurement SEP is comparable to the precision available using SEM characterization.

Measurement Technique:	2-θ			λ-scan		
Diffraction Order(s) Used:	0-order	1-order	0&1	0-order	1-order	0&1
Width SEP (nm) no noise	16	25	9	12	11	4
Width SEP (nm) noise in measurement	16	25	9	12	13	4
Width SEP (nm) noise in measurement & noise in calibration	16	25	9	12	13	5
Height SEP (nm) no noise	67	116	49	134	125	114
Height SEP (nm) noise in measurement	67	124	48	134	125	114
Height SEP (nm) noise in measurement & noise in calibration (nm)	67	148	49	134	125	114

Table 8. The SEPs (standard errors of prediction) for measuring critical dimensions of the 0.5/1.0 W deposition structure.

We applied the sub-range analysis described in Section 3.1 to improve the line height predictions. The height was divided into 5 overlapping sub-ranges between 0.0 μm and 1.0 μm, and the width was divided into 4 overlapping sub-ranges between 0.45 μm and 0.55 μm. The full-range results summarized in Table 8 were used to locate the prediction into one of the 20 "bins" corresponding to a particular combination of width and height sub-ranges. We then applied PLS to determine the SEP for each sub-range. We used 0-order and 1st-order data in which the measurement data and the calibration data had noise (i.e. the third noise situation).

Tables 9 and 10 summarize the line height SEP obtained for each of the 20 "bins" using the 2-Θ technique and the λ-scan technique, respectively. It can be seen that the height prediction was significantly improved to provide SEPs that are less than 5 nm for the λ-scan technique and less than 6 nm for the 2-Θ technique. We are very pleased with both of these results and consider both techniques capable of characterizing the 0.5/1.0 W structure..

Linewidth & Height Ranges	0.45 – 0.49 (μm)	0.47 – 0.51 (μm)	0.49 – 0.53 (μm)	0.51 – 0.55 (μm)
0.0 – 0.36 (μm)	0.0025 μm	0.0027 μm	0.0028 μm	0.0017 μm
0.18 – 0.54 (μm)	0.0040 μm	0.0051 μm	0.0047 μm	0.0045 μm
0.36 – 0.72 (μm)	0.0042 μm	0.0034 μm	0.0032 μm	0.0040 μm
0.54 – 0.90 (μm)	0.0026 μm	0.0025 μm	0.0025 μm	0.0031 μm
0.72 – 1.00 (μm)	0.0024 μm	0.0018 μm	0.0020 μm	0.0021 μm

Table 9. Sub-range analysis SEPs for line height prediction using unknown line width of the 0.5/1.0 W deposition structure. A 2-Θ measurement technique and both diffraction orders were used for the analysis.

Linewidth & Height Ranges	0.45 – 0.49 (μm)	0.47 – 0.51 (μm)	0.49 – 0.53 (μm)	0.51 – 0.55 (μm)
0.0 – 0.36 (μm)	0.0030 μm	0.0056 μm	0.0058 μm	0.0038 μm
0.18 – 0.54 (μm)	0.0030 μm	0.0022 μm	0.0019 μm	0.0030 μm
0.36 – 0.72 (μm)	0.0032 μm	0.0019 μm	0.0029 μm	0.0031 μm
0.54 – 0.90 (μm)	0.0028 μm	0.0028 μm	0.0026 μm	0.0028 μm
0.72 – 1.00 (μm)	0.0016 μm	0.0019 μm	0.0019 μm	0.0021 μm

Table 10. Sub-range analysis SEPs for line height prediction using unknown line width of the 0.5/1.0 W deposition structure. A λ-scan measurement technique and both diffraction orders were used for the analysis.

4.0 OVERLAY

Overlay is the measurement of registration of two adjacent layers to each other. Shrinking design geometries, coupled with increase in processing steps required for the manufacture of semiconductor devices, are placing an ever increasing demand on overlay tolerances. The overlay budget for 0.35 μm structures is 70 nm dictating the precision of the overlay measurement instrument to be 7 nm or better. This requirement decreases to 5 nm for 0.25 μm feature sizes. Optical microscopy techniques have been the dominant measurement technique to date, however, it is not clear that they will be able to meet the challenge as the feature size approaches 0.25 μm. The two major sources of error in overlay measurement are wafer induced shift, or WIS, due to overlay mark asymmetry, and tool induced shift, or TIS, due to measurement tool asymmetry. It is clear that in order to achieve overlay measurement precision of better than 5 nm any, and all, sources of error must be removed.

We proposed to test diffraction based techniques for overlay measurement and present the conclusion of our theoretical study. The structure under consideration is shown in Figure 8 and consists of a developed photoresist grating placed on top of an etched Si grating. The region in the space of this grating is filled with SiO_2. The periods of the two gratings are the same. The probe beam is from a He-Ne laser operating at 632.8 nm and a 2-θ scatterometer arrangement is used for obtaining the measurement. The diffracted power in both the +1 and -1 order beams is measured as the angle of incidence is scanned. The quantity of interest here is $K(\theta)$, which is the ratio of the power diffracted into the +1 order at an angle of incidence θ, to the power diffracted into the -1 order due to an angle of incidence of $-\theta$. Because the period of the two gratings is the same, they can be considered to be a single periodic structure and $K(\theta)$ is a measure of symmetry of this periodic structure.

In the absence of registration errors, the photoresist grating will be patterned exactly on top of the Si/SiO_2 grating, and a symmetrical periodic structure will be created. This will result in $K(\theta) = 1$ because the structure will appear the same at an angle of incidence equal to θ or $-\theta$. Registration errors in the patterning of the top photoresist grating will lead to an offset in the top grating as opposed to the bottom grating. This will create an asymmetry in the periodic structure which is shown in Figure 8. This will result in the deviation of $K(\theta)$ from 1. Figure 9 is a theoretical plot of $K(\theta)$ as a function of θ for different overlay errors. It can be seen that the curves differ significantly even for a small value of overlay error. Using the RCWT model we generated theoretical plots of $K(\theta)$ for overlay errors ranging from -40 nm to +40 nm with a step size of 5 nm. These plots were input into a PLS based calibration model, and an estimator of overlay errors was generated. The cross validated SEP of calibration was less than 0.5 nm, significantly less than the 5 nm requirement described previously.

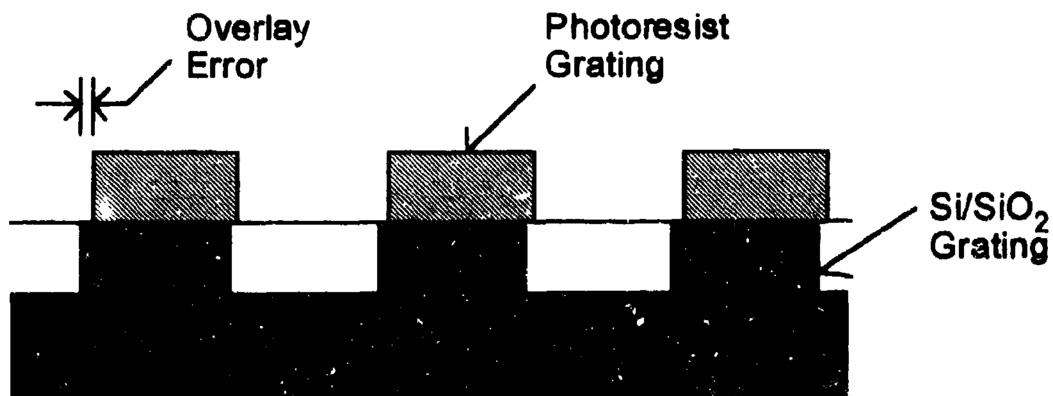

Figure 8: Illustration of the structure used to simulate application of scatterometry to monitor overlay, consisting of a Si/SiO_2 grating with a grating of photoresist on top and slightly displaced laterally.

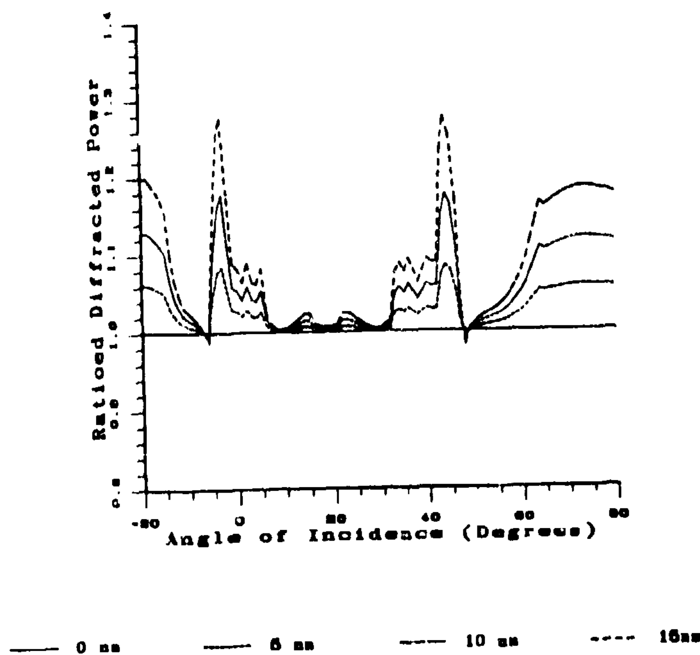

Figure 9: Plots of $K(\theta)$ versus angle of incidence for five different overlay errors illustrating the sensitivity of the scatterometry technique to monitor overlay.

5.0 INITIAL INSTRUMENT DESIGNS

Based on the results described above, two scatterometer configurations appear most feasible for applications to characterize line shapes in a cluster tool environment and overlay. One or both of these will be constructed in a Phase II effort as discussed in the next section.

Figure 10 illustrates an arrangement which represents a no-moving-parts version of the λ-scan scatterometer of Figure 3. Note that the materials involved in this system are vacuum compatible, and this permits locating the scatterometer in the load lock of a cluster tool system. A fiber optic directs white light to illuminate the sample. The 0-order component which is specularly reflected from the sample is directed back through the same fiber into a miniature spectrometer equipped with a 1024 element ccd detector array to provide rapid spectral resolution of this component. The detector arrays shown on both sides of the fiber characterize the higher-order diffraction from the sample. Different wavelength 1st-order diffraction components will illuminate different detectors on the arrays, thus providing spectral resolution. This arrangement neglects the overlap of a 1st-order component of one wavelength and a 2nd-order component of half the same wavelength. However, we do not see this to be a problem because of the statistical approach we are using for analysis and the fact that this "overlap" issue is repeatable. In addition, the 2nd-order terms typically are significantly less intense than the 1st-order terms and thus represent a minor changes to the signal levels involved.

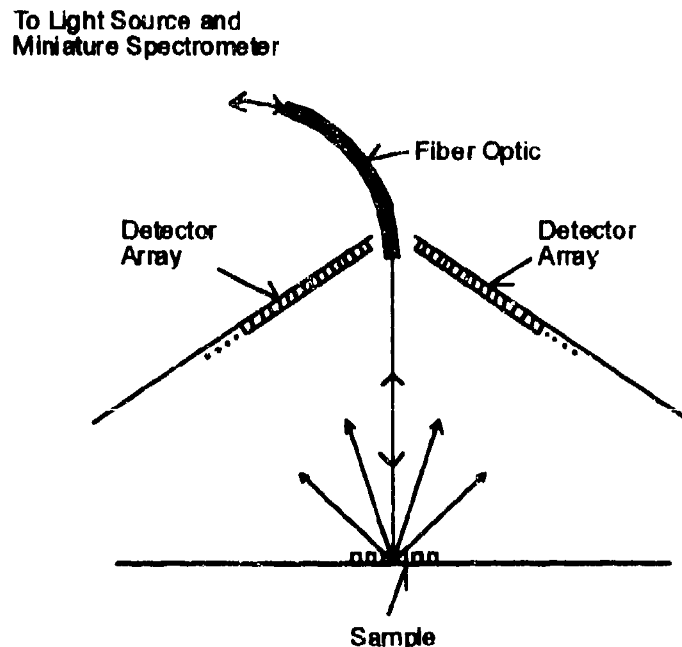

Figure 10: Arrangement of a no-moving-parts λ-scan scatterometer which is vacuum compatible.

The exact number of these detectors that is required is not known now, but we estimate 16 on each side of the fiber will be sufficient. This is based on collaborative work with AT&T in characterizing 0.5 μm pitch structures. In this work we obtained a complete data set of approximately 300 points to determine the lineshape of the structure and validated this with SEM characterization. We then performed analysis using fewer and fewer data points until the predicted lineshape began to differ from that predicted with the full data set. We found that 12 data points provided estimates of the lineshape that were effectively the same as the estimate obtained using the full data set.

Figure 11 illustrates a scatterometer configuration that is similar in principle to that of Figure 10, but which is appropriate for characterizing actual device patterns as opposed to line/space test patterns. In this arrangement the sample is illuminated with white light via a fiber, and the specularly reflected 0-order component is analyzed by the miniature spectrometer as before. The higher-order diffraction from the device pattern is directed through a lens to a color camera or an imaging spectrometer to provide a spectrally-resolved measurement of these components. Using a camera is simpler and faster, but it provides lower spectral resolution. Lower resolution may not be an issue because of the statistical analysis used; this would need to be investigated. The lens could be located inside the vacuum load lock of a cluster tool, and the remaining parts of the system would be in atmosphere.

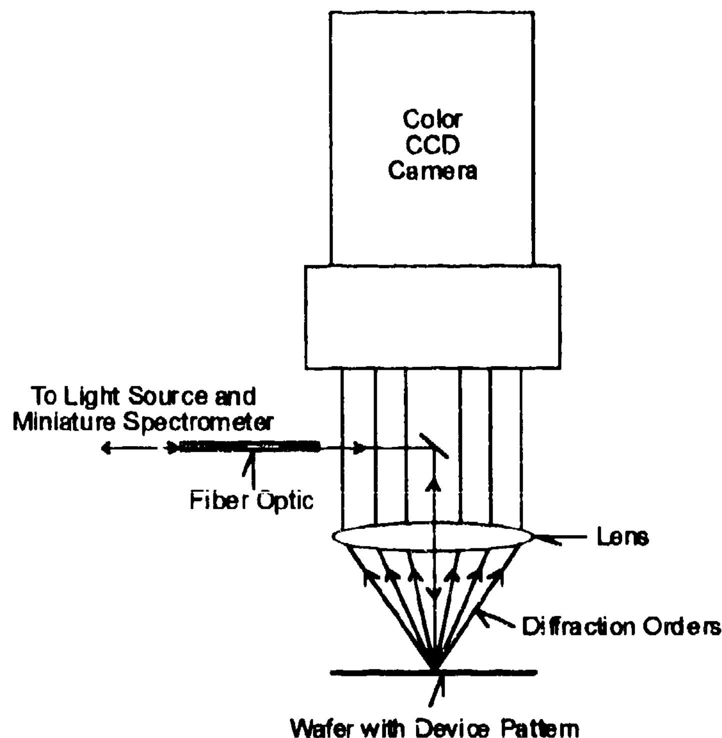

Figure 11: Arrangement of a no-moving-parts λ-scan scatterometer which can characterize device patterns.

Characterizing actual device patterns is more direct than characterizing line/space test patterns, and in this sense it is more appealing. However, it is not possible to model the two-dimensional diffraction from devices, and this precludes basing the technique on a firm theoretical background. In particular, training the statistical analysis technique would be based on an empirical approach in which diffraction from a number of samples is characterized, and the lineshape or overlay of the samples is also well characterized. The application also requires the pattern to have a high degree of periodicity, and this is often the case in advanced devices such as microprocessors and memory arrays. This approach has been used at the University of New Mexico to accurately characterize trench depths of 16 MB DRAM structures and planarization of SRAM device patterns.

6.0 CONCLUSIONS

We have shown that two scatterometry techniques can be applied to measure the line shapes of etched poly-Si and deposited W structures having 0.20 μm, 0.35 μm and 0.50 μm CDs with errors that are well within acceptable tolerance levels. These results can be improved using the sub-range technique described. In addition, overlay can be measured with less than 0.5 nm error.

Simulated scatterometer data was calculated using rigorous coupled wave diffraction theory. Analysis was performed using statistical techniques (PLS) to provide a simple method to determine the performance that can be expected from the scatterometer techniques. In addition, these simulation techniques represent a significant simplification compared to generating samples and characterizing them; this will be performed in a Phase II effort. We have used these same simulation techniques in similar applications in which experimental results were in close agreement with simulated results. These other results involved CDs between 0.12 μm to 2.0 μm.

This work has laid the foundation for developing more sophisticated scatterometer arrangements by showing the feasibility of the two basic techniques, 2-Θ and λ-scan, to measure lineshape and overlay. Using this background, more advanced systems can be designed and constructed to address specific issues, such as cluster tool applications.

7.0 PHASE II PLAN

We plan to propose a Phase II effort which will involve constructing scatterometers and implementing them on an etch or deposition reactor to pursue *in-situ* measurements. Presently we are having discussions with Sandia National Laboratories (SNL) and Lam Research in this regard. SNL is presently establishing the capability to process 0.5 μm geometries. However, smaller geometries would require *ex-situ* measurements using samples which would be obtained elsewhere. One possibility we are exploring is using e-beam written patterns in photoresist to fabricate smaller geometries with ion beam milling.

We will also involve the University of New Mexico as part of our Phase II effort because of their background in demonstrating scatterometer applications in microelectronics manufacturing. They will provide the modeling required for the fundamental understanding of processes as well as the optical expertise required.

APPENDIX 1: COPY OF REFERENCE 5

J. R. McNeil, S. S. H. Naqvi, S. M. Gaspar, K. C. Hickman, K. P. Bishop, L. M. Milner, R. H. Krukar, and G. A. Petersen, "Scatterometry applied to microelectronic processing," Microlithography World, pp. 16-22, Nov./Dec., 1992.

FEATURE

Scatterometry Applied to Microelectronics Processing

J.R. McNeil, S.S.H. Naqvi, S.M. Gaspar, K.C. Hickman, K.P. Bishop, L.M. Milner, R.H. Krukar, G.A Petersen
Center for High Technology Materials, University of New Mexico, Albuquerque, New Mexico

Scatterometry is a promising new optical metrology method for nondestructive rapid evaluation of many physical quantities of critical interest in microelectronics fabrication. Among these are latent image CDs in undeveloped resist, lithography tool focus and exposure parameters, etched structure CDs, photomask and phase shift mask characteristics, and metal grain sizes. This paper provides a general review of scatterometry, describes both instrumentation and methods, and introduces subjects to be discussed later in this series.

Critical dimensions (CDs) of 0.8 μm are common for high performance microelectronic devices. Advanced fabrication processes already involve CDs of 0.5 μm while technology for CDs of 0.35 μm and smaller is now being developed and the 0.1- to 0.2-μm range will be broached by early in the next decade. This trend, coupled with increasing automation and larger die and wafer sizes, only hints at the unprecedented demands now being made in the area of fabrication process control. With current CD error budgets typically 10% to 20% of the total CD, the absolute dimensional control required in fabricating advanced devices is 0.05 μm or smaller.

Unprecedented Process Control Demands an Unprecedented Metrology

Ideally, a metrology technique should be noncontact, nondestructive, rapid, quantitative, simple, and applicable in situ. An attractive alternative metrology technique that fits well with these objectives has appeared relatively recently. Called *scatterometry*, it is the angle-resolved characterization of light scattered from a surface. The method may be used for characterizing structure and topology as well as for controlling fabrication processes. It is noncontact, nondestructive, rapid, and quantitative, and in many cases can be used in situ. Scatterometry is useful in many areas, including microelectronics and the processing of optical elements and storage media. Its use can eliminate the need for optical microscope examination in many cases and, unlike microscopy, it is readily amenable to automated processing. In this article, we will review scatterometry applications that include characterization of photoresist latent images for exposure and focus control, etched structures, photomasks and phase shift masks, and Al-Si grain size.

Basic Principles

Scatterometry is a light scattering technique. Light scattering measurements have been used since the mid-1970s to characterize optical elements [1-4] in terms of the root mean square (*rms*) roughness. More recently, scatterometry has been applied to materials and processes used in microelectronics fabrication [6-9]. The method can characterize structures with dimensions much smaller than the wavelength λ of the light used. In contrast, optical microscopy has a spatial resolution comparable to λ.

Samples characterized by scatterometry have a periodic structure. This results from intentionally patterning the sample, or, alternatively, by considering a nominally smooth sample to be a superposition of many periodic structures as described below. Light which illuminates such a sample is diffracted at angles prescribed by the grating equation

$$\sin \Theta_i + \sin \Theta_s = n\lambda/d \qquad (1)$$

where Θ_i and Θ_s are the incident and scattered angles, respectively, n is an integer, and *d* is the period or pitch of the structure. With scatterometry, unlike imaging, the diffracted

Figure 1

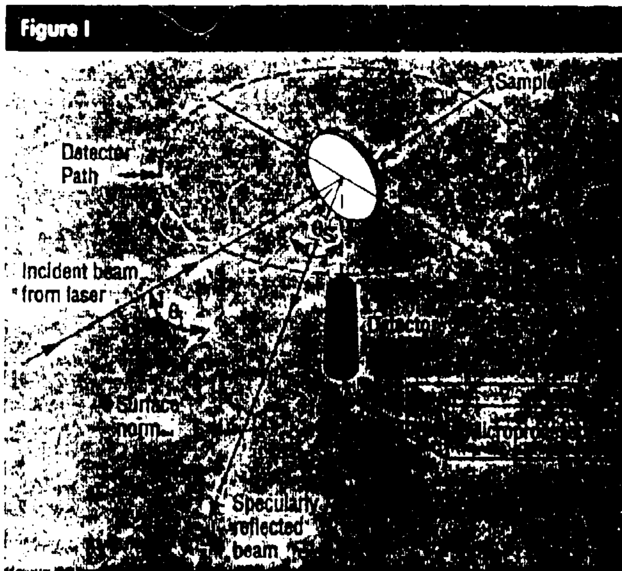

Exper ntal arrangement of a scatterometer

Figure 2

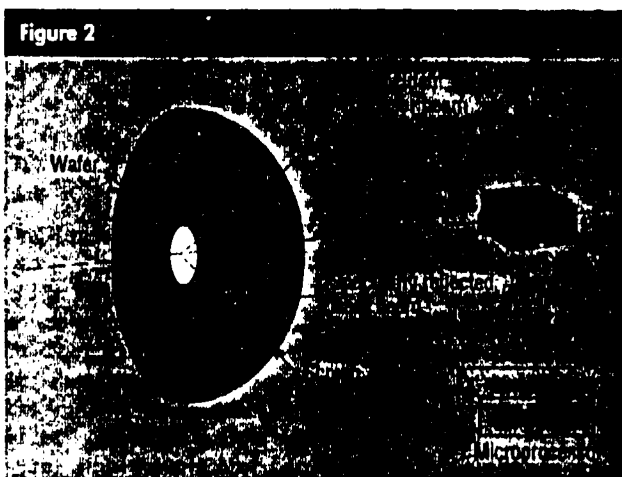

Scatterometer arrangement for characterizing two-dimensional scatter patterns

light is not combined or imaged prior to analysis. Instead, information about the lineshape of a sample is derived from the relative intensities of the different diffraction orders. From Eq (1), zero-order and 1st-order diffraction can occur for samples having a pitch slightly larger than λ/2. Thus, while the number of orders may be limited by λ, the lineshape information is limited only by the sensitivity with which small variations in the intensities of these orders can be detected. The greater the number of orders, the greater the information available but, as we shall see, much information can be gleaned from the zero order alone. Computer simulations suggest that scatterometry can be used in practice to characterize CDs as small as λ/20. Periodic test patterns are not necessarily required as many microelectronic devices have periodic structures which diffract light.

Experimental Arrangement

Figure 1 shows a basic scatterometer arrangement. The light

Figure 3

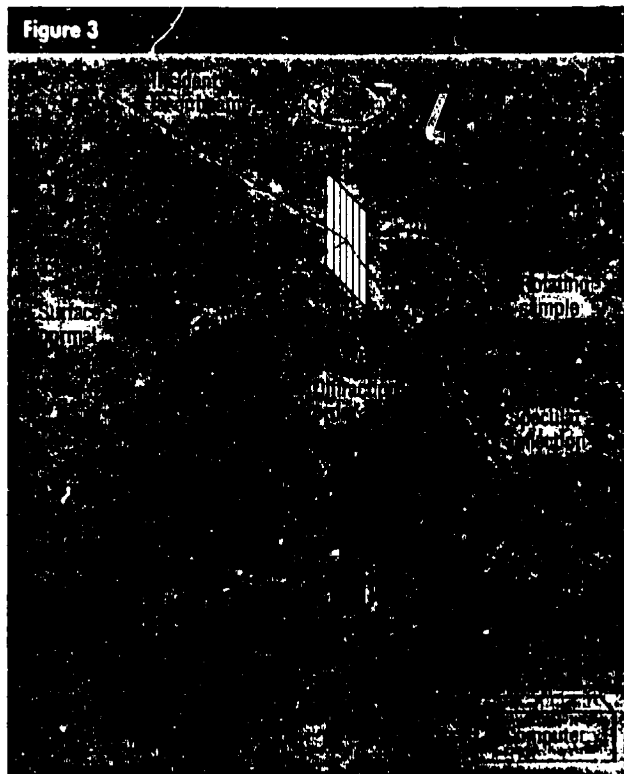

A "2Θ Scatterometer" arrangement especially suited for characterizing short pitch, small CD structures

source is usually a laser to simplify alignment and provide ample signal. Typically, the plane of polarization is perpendicular to the plane of incidence (s-polarized light) as this avoids surface plasma wave coupling in examining conducting samples. Often the laser output is spatially filtered to provide a well-defined spot at the sample. This is critical for allowing measurements close to the specularly reflected or directly transmitted beams. In addition, the polarization of the detected light can be analyzed using standard methods described in the literature [3-6].

Two dimensional scatter patterns are easily viewed using the arrangement of Fig. 2. Here the sample is placed at the center of curvature of a frosted dome and is illuminated so that the scatter pattern is displayed on the inside surface of the dome. A camera on the opposite side of the dome captures the image, a small computer is used for image processing and analysis, there are no moving parts, and measurements are rapid. Each spot of the pattern represents a diffraction order and contains information about the diffracting structure. Figure 3 illustrates another arrangement, which is well suited for characterizing short pitch, small CD structures. This "2Θ Scatterometer" has previously been employed by Zaidi, et al. [10] for grating characterization. Its use involves rotating the sample to continuously vary the angle of incidence. The detector rotates at a velocity such that the intensity of a specific diffraction order is continuously monitored, thus providing a large data set for that order.

A Theoretical Overview of Scatterometry

Diffraction From Periodically Patterned Surfaces

When an electromagnetic wave is incident on a surface, the light which is scattered is determined by the compositional

Figure 4

Diffraction characteristics for two periodic structures having the same pitch but different lineshape

Figure 5

Model data illustrates the dependence of 1st-order diffracted power on the linewidth of periodic structure having a 1.5-µm pitch. Conditions simulated were: Si substrate with 350 nm of SiO2, 1-µm photoresist, λ = 633 nm; beam TE polarized and incident at 30

properties (e.g., refractive index of the different regions) as well as the topographical characteristics (e.g., pitch, depth, and sidewall) of the surface. Properties of the incident beam (including wavelength, angle of incidence, and polarization) also determine the diffraction characteristics of the sample. Both the reflected and transmitted electromagnetic fields carry information about the scattering surface. Numerous metrology techniques (e.g., ellipsometry, optical microscopy, etc.) exploit this property of scattered fields to obtain compositional and/or topographical information about the scattering surface. When a periodic surface is illuminated, the scattered fields consist of distinct diffraction orders propagating in directions specified by the grating equation. This is shown schematically in Fig. 4, which illustrates the diffraction order intensities of two structures that have the same pitch but different linewidths.

The topographical dependence of diffraction is further illustrated in Fig. 5, which shows the calculated 1st-order diffraction intensity versus linewidth for a 1.5-µm pitch periodic photoresist structure. The sample was a 1.0 µm photoresist layer on 350 nm of SiO_2 on a Si substrate. The 633-nm beam was incident at 30° and was TE polarized. Diffraction characteristics plotted in the figure were calculated by direct solution of Maxwell's equations [11]. Details will be given in the last article of this scatterometry series.

Topology of "Smooth" Surfaces

The relation between electromagnetic scattering and smooth surface topology has been studied for many years, originally in connection with radar. In the case of a clean, perfectly reflecting surface where height variations are much smaller than the wavelength, the situation is simplified. Following Church's treatment [1,2] the sample is modeled as an infinite number of surfaces, each having structure with one spatial frequency and diffracting light at one angle according to Eq. (1). The surface is assumed to be sufficiently smooth such that only 1st-order diffraction is significant.

Vector scattering theories describe the differential light scatter dI_s as

$$\frac{1\,dI_s}{I_i\,d\omega_s} = \frac{C}{\lambda^4}\,Q(\Theta_i,\phi_i,\Theta_s,\phi_s,N,\chi_i,\chi_s)\,P(p,q) \qquad (2)$$

where C is a constant, I_i is the intensity of the incident light, and $d\omega_s$ is the solid angle of the detection system. The quantity Q in Eq. (2), called the "optical factor", is independent of the surface structure and is a function of the angles of incidence (Θ_i, ϕ_i), scatter angles (Θ_s, ϕ_s), complex index of refraction N of the surface, and polarization states of the incident and scattered light, χ_i and χ_s, respectively. The "surface factor" P(p,q) is the power spectral density (PSD) of the surface roughness. This is the output of the scatterometer measurement and is the function that describes the surface structure.

If the surface is in the X-Y plane, and $Z(X,Y)$ is the surface height variation relative to that plane, the PSD is given by

$$P(p,q) = \frac{1}{A}\left|\frac{1}{2\pi}\iint dxdy\; e^{i(px+qy)}\,Z(x,y)\right|^2 \qquad (3)$$

where A is the area illuminated, and p and q are the surface spatial frequencies in the X and Y directions, respectively. In other words, the PSD is the average squared magnitude of the two-dimensional Fourier transform of the surface roughness.

It is convenient to describe the surface roughness in terms of the *rms* roughness σ, which is given in terms of the instrument bandwidth and modulation transfer function (MTF), M(p,q) as

Different values of σ will result if the integral limits (i.e.,

$$\sigma^2 = \int_{p_{min}}^{p_{max}} dp \int_{q_{min}}^{q_{max}} dq\; M(p,q)P(p,q) \qquad (4)$$

bandwidth) or MTF in the integral change. If *rms* roughness values from examining the same surface using different instruments are to be compared, the bandwidths and MTFs should be the same [4]. In the case of an isotropic surface st[illegible]re, p and

Figure 6

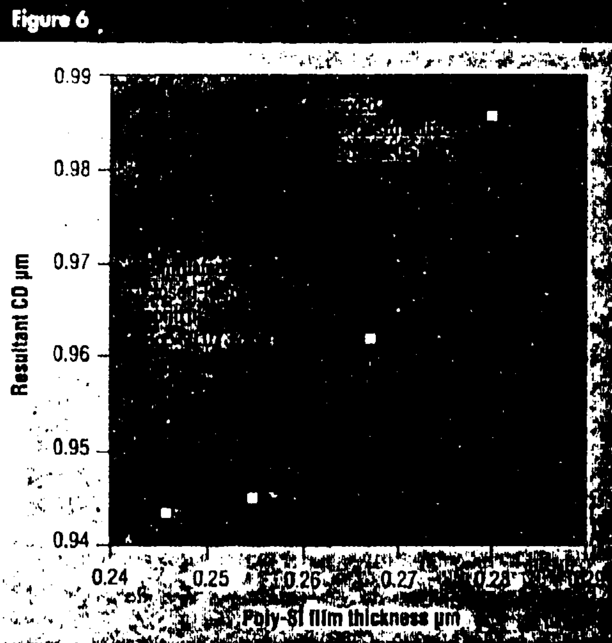

Changes in developed photoresist CD resulting from variations in underlying poly Si film thickness. The scatterometer-controlled exposure dose provided nearly a factor of four improvement in CD control compared to using fixed exposure time. The linewidth and period were nominally 1 µm and 2 µm, respectively.

q are identical, and only one of the spatial wavelengths is needed to describe the lateral dimension of sample structure.

Applications Overview

A review of scatterometry applications is presented here. Further details will appear in subsequent articles of this series. For applications in microelectronics, sample surfaces can be a test pattern or part of the device being fabricated. The illuminating spot can be as small as 30 µm ($1/e^2$ diameter), so that a minimum of ten or so lines of the periodic structure are illuminated [6]. Such a small test pattern can be located in the scribe lines of the wafer.

Photoresist Latent Image Characterization

In lithography, exposure and focus are but two of the variables that control the shape of the developed photoresist pattern. Baking subsequent to exposure also influences the resulting shape of the developed resist and thus represents an additional variable which must be accounted for in process evaluation. It is preferable to decouple these effects and independently determine the appropriate process window for each of the exposure, bake, and develop steps. Scatterometry can be used effectively in this regard to monitor the latent image prior to bake and develop.

In photoresist, a latent image is formed as the photoactive compound (PAC) concentration changes upon exposure. A grating on the photomask can generate a resist pattern with a periodic PAC concentration profile that diffracts light when illuminated [12,13]. The diffraction characteristics of latent image gratings can be rigorously modeled. First, lithography simulation tools such as SAMPLE [14] and PROLITH [15] are used to predict the PAC concentration inside the photoresist as a function of exposure conditions (dose, focus) and substrate and resist parameters (thickness, composition). Then, rigorous coupled wave theory [16] is employed to predict the amount of incident probe beam power diffracted into the various orders.

Figure 7

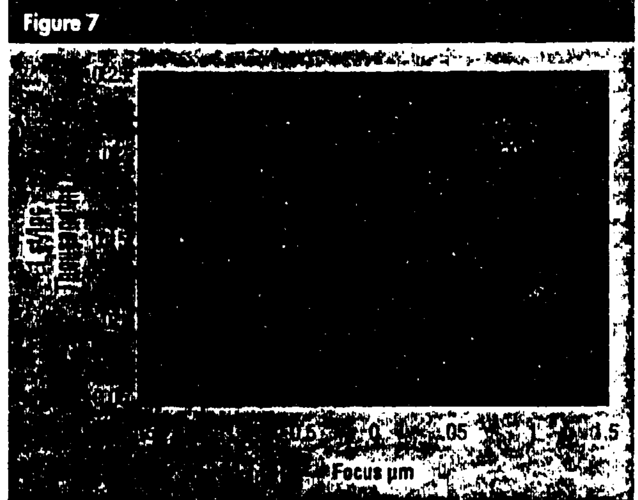

Variation of 1st-order diffraction intensity from a photoresist latent image for different stepper focus conditions

A significant problem occurs in optical lithography because the exposure dose is a function of the underlying film structure. Since the underlying films can vary from lot to lot, wafer to wafer, or even die to die on a wafer, the use of fixed exposure time (dose) — the present technique used for CD control — can adversely affect critical dimension control. By using scatterometry to monitor the latent image, CD variations can be reduced [6,9,12] by nearly four times (Fig. 6). These results are applicable to any transparent film material; poly Si was used in this work to provide the electrical measurements necessary for CD verification.

Diffraction from latent image gratings can also be used to determine optimal focus conditions. Theoretical simulations have shown [9] that, for any exposure dose, the power diffracted into the 1st order is at a peak for optimal focus conditions, regardless of the composition of layers underneath the photoresist. This was first demonstrated experimentally by Adams [13]. Milner et al. [9] established that, for the case of photoresist on crystalline Si, the 1st- and 2nd-order diffraction intensities reach maxima at optimal focus. However, recent experimental results for photoresist on α-Si and poly-Si show that, while the 1st-order intensity always peaks at optimal focus, the 2nd order intensity is dependent upon the underlying layers and may or may not peak at optimal focus. Thus, it is important to distinguish between the various diffracted orders and detect each of them separately.

Figure 7 illustrates experimental and theoretical 1st order intensity variation versus focus for photoresist on α-Si. The zero defocus position is at the top of the photoresist. The difference between the peak location of the two curves is believed to be due to an error in the ability of the stepper to locate the top of the photoresist. Subsequent SEM measurements of the developed photoresist gratings indicated that the optimal focus location was at 0.1 µm, the same as the peak of the experimental curve in the figure.

Figure 8

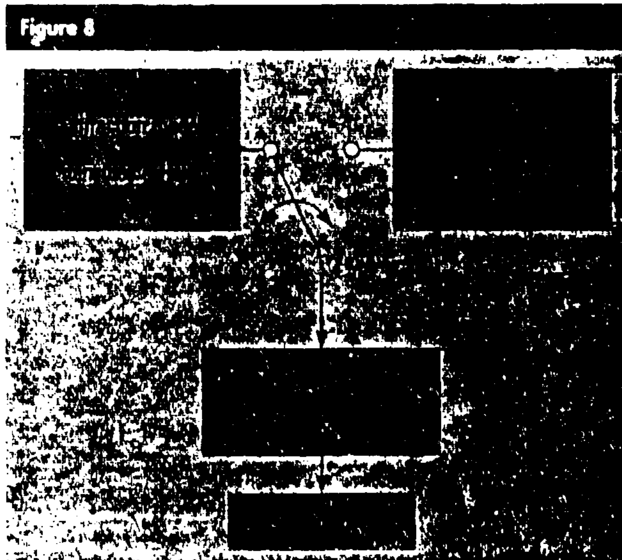

Analysis strategy used to predict sample etch depth, theoretical scatterometer data were used to train statistical techniques and experimental scatterometer data were subsequently input to predict the depth of a sample

Figure 9

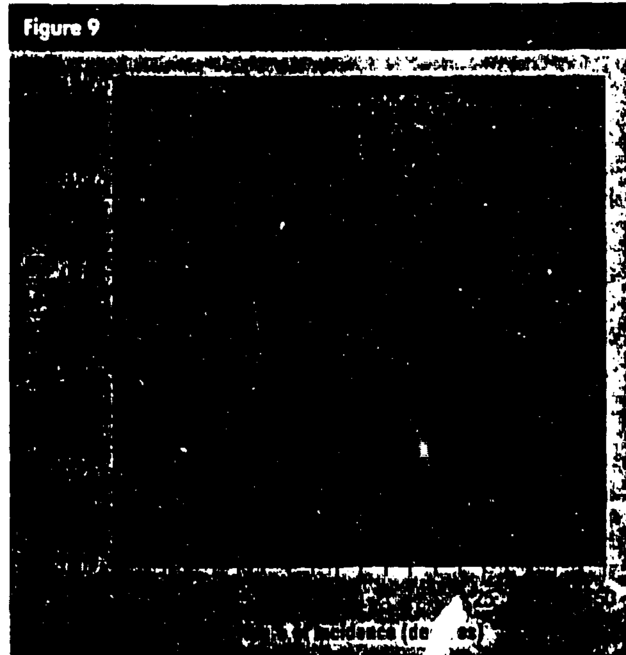

Model and experimental data for the zero-order diffraction intensity from a line structure with a 10-μm pitch, 5-μm width, and 0.371-μm depth measured using the "2Θ Scatterometer" arrangement

Scatterometry for Etched Structure Characterization

Scatterometry can be used to analyze etched structures rapidly and nondestructively [17-18]. One example of scatterometer characterization of the depth of an etched structure involved patterns that had 32-μm pitch and 1.5-μm wide lines etched in crystalline Si. Due to the large pitch, the diffraction patterns from these structures contained many orders, and the intensity of each order was sensitive to the depth of the lines. Statistical techniques were used to analyze the patterns, as illustrated schematically in Fig. 8. The goal was to predict the etch depth from the scatter characteristics. Procedurally, this involved the use of a neural network and a partial least squares method [19-21]. First, the coupled wave model generated a set of theoretical data that was used for calibration and for "training" the statistical techniques. Then, experimental data from the scatterometer measurements was input to the statistical operations to predict the sample depth. Results were very good. For fourteen samples, each nominally 900 nm in depth, the neural net prediction had an average error of 8.8% ± 4.06%, or 80 nm ± 37 nm. The partial least squares prediction tightened this to an average error of 0.8% ± 0.3%, or 7 nm ± 3 nm. Sample depths were verified using a scanning force microscope (SFM), which had an error of approximately 1%. It was not necessary to fabricate and characterize calibration samples. The calibration data that were generated from the model are based on Maxwell's equations and rigorous diffraction theory and thus can be considered absolutely accurate. This same approach can be extended to predict sidewall characteristics.

Chrome-on-Glass Photomask Grating Metrology

Accurate linewidth metrology of photomasks is essential for production of devices with feature sizes less than 0.5 μm. A NIST (US National Institute of Standards and Technology) linewidth standard now exists for 0.9 μm lines of chrome on glass. However, linewidth standards are nonexistent for smaller CDs of chrome on glass or any other material, for that matter.

Scatterometry provides a simple and accurate method for determining linewidths of photomask gratings. In this application, an incident laser beam produces a scattered field consisting of multiple reflected and transmitted orders. A simplified scalar model of diffraction indicates that the amount of power diffracted into the transmitted zero order should be inversely proportional to the linewidth. The linewidth of the photomask grating may be predicted, therefore, from a measurement of intensity of the transmitted zero order [8]. To rigorously establish this inverse relationship, the chrome on-glass grating may be modeled as an 80-nm thick chrome layer deposited on a glass substrate with an 18-nm thick antireflecting layer of chrome oxide. Application of rigorous coupled wave theory [16] confirmed a monotonic relationship between the linewidth of the grating and the transmitted zero order power. A "lookup table" can be used to give the linewidth for a measured zero-order intensity.

Experiments verified that the linewidth obtained with scatterometry was comparable to that obtained using other optical metrology instruments. One mask having six different submicron linewidth gratings was sent to several companies to determine instrument-to-instrument variation in CD measurements. No consensus was obtained for the linewidth values using the different instruments. Scatterometry provided CD measurements that were comparable to those obtained using the various metrology instruments. In some cases, the results differed by less than 5% (e.g., results from a Nanoline IIIB). The long term (18 mos.) repeatability of the measurements was found to be approximately 96%.

Line Edge Roughness

Mask patterns can have both random structure and periodic error on line edges. The former produces an isotropic, diffuse

Figure 10

Power spectral density (PSD) characteristics of Al-Si material deposited on Si wafers at different deposition temperatures.

scatter and the later produces diffraction, both of which are superimposed on the diffracted pattern of the desired line structure. These two undesirable components of scattered light can be treated separately, but preliminary work has focused on a differential measurement technique that includes both.

The dome technique of Fig. 2 was used to measure the two-dimensional scatter from mask patterns that nominally have a one-dimensional periodic structure. For example, perfect structure on the mask would diffract through a diameter of the dome at several points determined by the number of diffraction orders that occur. For each measurement, the data are transferred to a computer and image processing techniques subtract the ideal diffraction pattern from the experimentally obtained pattern. The contribution of the residual scatter is integrated and normalized to the integral of the total scatter in the experimental pattern. This defines a figure of merit (FOM) as

$$FOM = \left[\frac{\int \text{Scattered light exclusive of ideal diffraction}}{\int \text{All scattered light}} \right]^{-1}$$

Three photomasks were examined: one which had good quality lines, one that had a sinusoidal edge structure intentionally superimposed on the line edges, and one that was intentionally etched to produce significant line edge roughness. The resulting FOM values for the masks were 3.57, 3.03, and 2.56, respectively, suggesting that scatterometry is a promising quantitative technique for mask characterization.

Phase Shift Masks

Phase shift photomasks have recently attracted a great deal of attention. Selective changes in the phase of the light as it traverses the phase mask improves the resolution of the imaged lines which are printed. Accurate measurement of the phase shifts resulting from thickness variations is presently a problem. In line with this, mask structures were examined using the "2Θ Scatterometer." The results are illustrated in Fig. 9. Experimental and model results are plotted for the zero-order intensity diffracted from a 10-µm pitch, 5-µm linewidth structure, which was ion beam milled to a depth of approximately 0.37 µm. The angle of incidence was varied over ± 50°. The dip in the solid curve at 0° results from the detector blocking the incident beam. The difference between the experimental and modeled curves is 2.3%. Modeled data for other depths indicate that the variation of the zero-order light intensity is quite sensitive to the etched depth.

Nominally "Smooth" Surfaces

Figure 10 illustrates the power spectral density characteristics for five samples (courtesy of Intel) of Al-Si alloy material, which were deposited at different substrate temperatures between ambient and approximately 350°C. The area under the PSD curves increases and the secondary peaks shift to lower spatial frequencies (higher spatial wavelengths) as temperature increases. The area increase is indicative of increasing sample roughness, as expected, and the peak shift is indicative of increased grain size of the material. Using SEM techniques to determine grain size, consistent results were obtained when compared to *rms* roughness (98% correlation), although the SEM characterization required the samples to be broken and etched. Similar results have been observed for Al-Cu and Al-Si (from other manufacturers) deposited at different substrate temperatures, levels of substrate bias, and with antireflection (AR) layers. Samples of Al have also been characterized using grating coupling to surface plasma waves to determine the electrical properties of the films [22]. This application of scatterometry is compatible with the industry trend to build characterization directly into sputter systems or cluster tool arrangements.

In a similar manner, we have characterized other materials including CVD W and silicides. For example, the effect of oxide growth on the surface properties of WSi_2 is easily detected using scatterometry. The as-deposited material is smooth, and the PSD peaks at small spatial wavelengths, outside the measurement bandwidth of the scatterometer. Subsequent oxidation of the surface at elevated temperatures promoted grain growth in the material. The *rms* roughness of the sample increased by a factor of four, and the sample PSD plot peaked at large spatial wavelengths (5 µm). This is consistent with results from microscopic examination of the samples.

Conclusions and Forecast of Future Applications

The scatterometry applications reviewed above illustrate the technique's wide range of applicability in providing a nondestructive, rapid, quantitative process monitor. Although the applications discussed range from lithography control to etched structure monitoring to metal grain size determination, these only begin to utilize the technique's capability. Measurements can also be performed using multiple wavelengths and polarizations to yield even greater information. As a dimensional metrology tool, scatterometry will meet industry requirements well into the future. Visible light enables scatterometry characterization of structures that have 0.15-µm CDs and smaller; use of ultraviolet sources can extend these limits even further.

Scatterometers of the form shown in Fig. 1 are commercially available from TMA Technologies, Bozeman, MT. In addition,

scatterometers illustrated in Figs. 1,2, and 3 are supplied on a custom basis by Sandia Systems Inc., Albuquerque, NM.

Acknowledgment

This work was funded in part by SEMATECH The authors gratefully acknowledge useful conversations and assistance from S.R.J. Brueck, S.H. Zaidi, J.E. Franke, and T.M. Niemczyk of the University of New Mexico; D.M. Haaland, B.L. Draper, G.D. Tipton, and B.R. Stallard of Sandia National Laboratories, Albuquerque, NM; S.R. Wilson of Sandia Systems Inc., Albuquerque, NM; Y.E. Strausser of Surface Sciences Laboratories, Mountain View, CA; B.R. Mariacher of SEMATECH; and R.A. Gottscho of AT&T Bell Laboratories. The partial least squares analysis discussed above was the result of joint activity with Franke, Niemczyk, and Haaland. ■

References

1. E.L. Church, H.A. Jenkinson, J.M. Zavada, "Relation Between the Angular Dependence of Scattering and Microtopographic Features," *Opt. Eng.*, vol. 18, p. 125 (1979).
2. E.L. Church, J.M. Zavada, *Appl. Opt.*, vol. 14, p. 1788 (1975).
3. J.C. Stover, "Optical Scattering: Measurement and Analysis," McGraw-Hill, New York, NY, 1990.
4. R.D. Jacobson, S.R. Wilson, G.A. Al-Jumaily, J.R. McNeil, J.M. Bennett, "Microstructure Characterization by Angle-Resolved Scatter and Comparison to Measurements Made by Other Techniques," *Appl. Opt.*, vol. 31, p. 1426 (1992).
5. J.R. McNeil, S.S.H. Naqvi, S.M. Gaspar, K.C. Hickman, S.R. Wilson, "Optical Scatterometry," to be published in the *Encyclopedia of Materials Characterization*, Charles Evans, Richard Brundle, Shaun Wilson, eds., Manning Publications Co., 1992.
6. K.C. Hickman, S.M. Gaspar, K.P. Bishop, S.S.H. Naqvi, J.R. McNeil, "Use of Light Scatter From Latent Images to Improve Lithography Control," to be published in *J. Vac. Sci Technol.*
7. P.G. Konstantinos et al.,"Use of Light Scattering in Characterizing Reactively Ion Etched Profiles," *J. Vac. Sci. Technol.*, vol. A9(3), p. 664 (1991).
8. S.S.H. Naqvi, S. Gaspar, K. Hickman, K. Bishop, J.R. McNeil, "Linewidth Measurement of Gratings on Photomasks: A Simple Technique," *Appl. Opt.*, vol. 31, p. 1377 (1992).
9. K.P. Bishop, L.M. Milner, S.S.H. Naqvi, J.R. McNeil, "Use of Scatterometry for Resist Process Control," *Proceedings of the SPIE*, vol. 1673, "International Circuit Metrology, Inspection, and Process Control VI," M.T. Postek, ed., p. 441 (1992); see also L.M. Milner, K.C. Hickman, S.M. Gaspar, K.P. Bishop, S.S.H. Naqvi, J.R. McNeil, "Latent Image Exposure Monitor Using Scatterometry," *ibid.*, p. 274.
10. S.H. Zaidi, M. Yousaf, S.R.J. Brueck, "Grating Coupling to Surface Plasma Waves. I. First-Order Coupling," *J. Opt. Soc. Am.*, vol. B8, p. 770 (1991); see also S.H. Zaidi, M. Yousaf, S.R.J. Brueck, "Grating Coupling to Surface Plasma Waves. II. Interactions Between First- and Second-Order Coupling," *J Opt. Soc. Am.*, vol. B8, p. 1348 (1991).
11. K.P. Bishop, S.M. Gaspar, L.M. Milner, S.S.H. Naqvi, J.R. McNeil, "Grating Lineshape Characterization Using Scatterometry," *Proceedings of the SPIE*, vol. 1545, "International Conference on the Application and Theory of Periodic Structures," J.M. Werner, W.R. McKinney, eds., p. 64 (1991).
12. K.C. Hickman, S.M. Gaspar, K.P. Bishop, S.S.H. Naqvi, J.R. McNeil, "Use of Diffracted Light from Latent Images to Improve Lithography Control," in "Integrated Circuit Metrology, Inspection and Process Control V," SPIE vol. 1464, p. 245 (Mar. 1991).
13. T.E. Adams, "Applications of Latent Image Metrology in Microlithography," *ibid.* p. 294.
14. C. A. Mack, "PROLITH: A Comprehensive Optical Lithography Model," in "Optical Microlithography IV ," SPIE vol. 538, p. 207 (1985).
15. W.G. Oldham, S.N. Nandgaonker, A.R. Neureuther, M. O'Toole, "A Generalized Simulator for VLSI Lithography and Etching Processes: Part I – Applications to Projection Lithography," *IEEE Trans. Elec. Dev.*, vol. 26, p. 717 (1979).
16. M.G. Moharam, T.K. Gaylord, "Rigorous Coupled-Wave Analysis of Metallic Surface-Relief Gratings," *J. Opt. Soc. Am.*, vol. A3, p. 11 (1986).
17. K.P. Giapis et al., *J. Vac. Sci. Technol.*, vol. A9, p. 664 (1991); see also R. H. Krukar, A. Kornblit, L.A. Clark, D.L. Lambert, J. Kruskal, E.A. Reitman, R.A. Gottscho, *J. Appl. Phys.* (submitted).
18. R.H. Krukar et al., *Digest, Optical Society of America Annual Technical Meeting*, Washington, DC, vol. 23, p. 204 (1992).
19. D.E. Rumelhart, J.L. McClelland, *Parallel Distributed Processing: Explorations in the Microstructure of Cognition: Foundations*, vol. 1, MIT Press, Cambridge, MA (1986).
20. D.M. Haaland, E.V. Thomas, "Partial Least-Squares Methods for Spectral Analyses. 1. Relation to Other Quantitative Calibration Methods and the Extraction of Qualitative Information," *Anal. Chem.*, vol. 60, p. 11 (1988).
21. E.V. Thomas, D.M.Haaland, "Comparison of Multivariate Calibration Methods for Quantitative Spectral Analysis," *Anal. Chem.*, vol. 62, p. 1091 (1990).
22. S.H. Zaidi, D.W. Reicher, B.L. Draper, J.R. McNeil, S.R.J. Brueck, "Characterization of Thin Al Films Using Grating Coupling to Surface Plasma Waves," *J. Appl. Phys.*, vol. 71, p. 6039 (1992).

John R. McNeil received his B.S. and M.S. degrees in Physics from the University of Texas at Austin in 1964 and 1971, respectively, and his Ph.D. degree in Electrical Engineering from Colorado State University in 1977. He is presently a professor of Electrical Engineering and is associated with the Center for High Technology Materials at the University of New Mexico. His research interests include development of metrology techniques for semiconductor processing using light scatter techniques, as well as optical component and thin film fabrication processes.

S. Sohail H. Naqvi was born in Wah Cantt, Pakistan, in September 1962. He received his B.S.E.E. with highest distinction, and his M.S.E.E. and Ph.D. degrees in 1984, 1986, and 1988, respectively, all from Purdue University. He joined the faculty of the University of New Mexico after graduation where he is now with the Center for High Technology Materials and an assistant professor in the Department of Electrical and Computer Engineering. His research interests lie in optical communications, diffractive optics, and electromagnetic wave diffraction theory with application towards development of diffraction-based semiconductor metrology techniques.

Susan M. Gaspar received her B.S. in Physics from the University of Arizona in 1988, and her M.S.E.E. from the University of New Mexico in 1992. She is currently pursuing her Ph.D. in Electrical Engineering at UNM while also a research assistant at the Center for High Technology Materials. Her research interests include phase shifting masks, inverse scattering, and use of diffraction from gratings for process control.

Kirt C. Hickman received his B.S.E.E. from the University of New Mexico in 1989. He received his M.S.E.E. in Optoelectronics in 1991, also from UNM. He is currently doing research on scatter from optical materials and coating at Phillips Laboratory in Albuquerque, New Mexico.

Kenneth P. Bishop received his B.S.E.E.T. from DeVry Institute of Technology in Atlanta, GA in 1988. He received his M.S.E.E. from the University of New Mexico in 1992. He is currently working in optical propagation for Applied Technology Assoc. in Albuquerque, New Mexico.

Lisa-Michelle Milner received her B.S.E.E. from the University of New Mexico in 1991. She is working as a research assistant at the Center for High Technology Materials while pursuing a M.S.E.E. at the University of New Mexico. Her current research interests include the use of grating diffraction to monitor and optimize the focus and exposure conditions for optical lithography.

Richard H. Krukar received his B.U.S. and M.S.E.E. degrees from the University of New Mexico and is presently completing the requirements for the Ph.D. degree there. He has worked and consulted in the computer industry for over ten years, with recent work involving optical scatter applications.

Gary A. Petersen received his B.S. in Physics from Rensselaer Polytechnic Institute in Troy, NY, in 1989, and his M.S.E.E. from the University of New Mexico in 1991. He is presently pursuing a Ph.D in Electrical Engineering at UNM. His current research interest is CVD metals, primarily CVD copper for microelectronics applications.

Distribution

Commander U.S. Army Missile Command ATTN: AMSI-RD-WS-DP-SB (Mr. Savage, Tech Monitor) Bldg 7770, Room 101G Redstone Arsenal, AL 35898-5248	2 Copies
Commander U.S. Army Missile Command ATTN: AMSI-RD-CS-R Redstone Arsenal, AL 35898-5280	1 Copy
Defense Intelligence Agency Missile & Space Intelligence Center ATTN: MSC-2D Redstone Arsenal, AL 35898-5500	1 Copy
Commander U.S. Army Missile Command ATTN: AMSI-RD-WS Redstone Arsenal, AL 35898-5248	1 Copy
Director Defense Advanced Research Projects Agency ATTN: MTO (Mr Lemnios) 3701 North Fairfax Drive Arlington, VA 22203-1714	1 Copy
Director Defense Advanced Research Projects Agency ATTN: TIO 3701 North Fairfax Drive Arlington, VA 22203-1714	1 Copy
Defense Technical Information Center ATTN: DTIC-DDR Alexandria, VA 22304-6145	2 Copies

DEFENSE ADVANCED RESEARCH PROJECTS AGENCY
3701 NORTH FAIRFAX DRIVE
ARLINGTON, VA 22203-1714

November 20, 2001

Ms. Kelly Akers
Defense Technical Information Center
8725 John J. Kingman Road
Suite 0944
Ft. Belvoir, VA 22060-6218

Dear Ms. Akers:

This is to advise you that the following documents have been reviewed and/or declassified and released under the Freedom of Information Act.

- Document Number: AD 803668
  Unclassified Title: Sailwing Wind Tunnel Test Program
  Report Date: September 30, 1966

- Document Number: AD 461202
  Unclassified Title: XV-8A Flexible Wing Aerial Utility Vehicle
  Report Date: February 1, 1965

- Document Number: AD 460405
  Unclassified Title: XV-8A Flexible Wing Aerial Utility Vehicle
  Report Date: February 1, 1965

- Document Number: AD 431128
  Unclassified Title: Operational Demonstration and Evaluation of the Flexible Wing Precision Drop Glider in Thailand
  Report Date: March-July 1963

- Document Number: AD 594 137L
  Unclassified Title: Communist China and Clandestine Nuclear Weapons-Input Substudies A-J, SRI Report
  Report Date: October 1970

- Document Number: AD B 176711
  Unclassified Title: Overlay and Grating Line Shape Metrology Using Optical Scatterometry
  Report Date: August 31, 1993

If you have any questions, please contact Mr. Fred Koether, our Declassification Specialist, at (703) 696-0176.

TELCON, 4 DEC 2001, MR. KOETHER STATED THAT ABOVE DOCUMENTS ARE APPROVED FOR PUBLIC RELEASE
Tony Nourany

Sincerely,

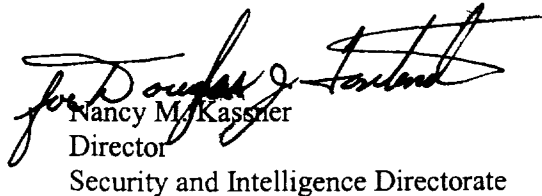

Nancy M. Kassner
Director
Security and Intelligence Directorate